





# Coupling between the Magnetospheric Dipolarization Front and the Earth's Ionosphere by Ultralow-frequency Waves

Pengfei Qin<sup>1,2,3</sup> , Yasong Ge<sup>1,2,3,6</sup> , Aimin Du<sup>1,2,3</sup>, Can Huang<sup>1,2,3</sup>, Ying Zhang<sup>1,2,3</sup>, Hao Luo<sup>1,2,3</sup>, Jiaming Ou<sup>1,2,3</sup>, Tielong Zhang<sup>4,5</sup>, and Lican Shan<sup>1,2,3</sup>

<sup>1</sup> Key Laboratory of Earth and Planetary Physics, Institute of Geology and Geophysics, Chinese Academy of Sciences, Beijing, People's Republic of China  
[ysge@mail.iggcas.ac.cn](mailto:ysge@mail.iggcas.ac.cn)

<sup>2</sup> Innovation Academy for Earth Science, Chinese Academy of Sciences, Beijing, People's Republic of China

<sup>3</sup> University of Chinese Academy of Sciences, Beijing, People's Republic of China

<sup>4</sup> Harbin Institute of Technology, Shenzhen, People's Republic of China

<sup>5</sup> Space Research Institute, Austrian Academy of Sciences, Graz, Austria

Received 2020 April 14; revised 2020 April 28; accepted 2020 April 29; published 2020 May 20

## Abstract

Magnetosphere–ionosphere coupling is representative of a class of astrophysical problems involving the interaction between very different plasma regimes that are connected by magnetic fields. It is a major issue of the planet's (e.g., Earth, Jupiter, Saturn) system how the magnetospheric plasma is coupled to the planet's ionosphere/atmosphere. Due to their roles on energy transport and conversion in the terrestrial magnetosphere, dipolarization fronts (DFs) in the magnetotail have been intensively studied. While the energy may also be transported toward the ionosphere during the magnetosphere–ionosphere coupling, the coupling processes during DF events remain unclear. Using high-quality MMS and Swarm measurements, we present new conjugated observations of ultralow-frequency waves associated with the DF in the magnetotail and multiscale field-aligned currents (FACs) in the ionosphere. The tail large-amplitude low-frequency magnetic disturbances and associated FACs were found connected with a pair of ionospheric FACs near the magnetic footprints of MMS. The earthward field-aligned Poynting flux of low-frequency waves reveals the energy transport from the DF toward the ionosphere. Meanwhile, small-scale and highly temporal ionospheric FACs suggest that the magnetotail shear Alfvén waves may evolve into kinetic Alfvén waves during the coupling processes. This finding implies that a very localized dynamic process (e.g., DFs in the terrestrial magnetotail) in the magnetosphere could couple the ionosphere with Alfvén waves.

*Unified Astronomy Thesaurus concepts:* [Earth \(planet\)](#) (439); [Alfvén waves](#) (23); [Geomagnetic fields](#) (646)

## 1. Introduction

A class of astrophysical problems involve the interaction between very different plasma regimes that are connected by magnetic fields (Mauk et al. 2002). Such a process is required and commonly seen in the interaction between planets and planetary moons (Delamere 2003; Saur et al. 2004; Tsurutani et al. 2020), the coupling of the planetary magnetosphere and ionosphere (Mcpheeron et al. 1973; Cowley 2000; Russell et al. 2000), and the coupling of the planet's magnetosphere and atmosphere (Anderson et al. 2014). A pair of large-scale currents along the magnetic field (field-aligned current, FAC) of Jupiter connect the Jovian ionosphere with its closest moon Io and Io's torus, transferring energy and momentum between the planet and Io in the form of an Alfvén wave (e.g., Saur et al. 2004). These interaction processes (FACs or Alfvén waves) are usually associated with the generation of auroral activities on the planetary ionospheres across the solar system, which are important indicators of magnetospheric processes (Bagenal 2007). It was theoretically proposed that localized disturbances can affect the behavior of an entire cosmical plasma system via FACs or Alfvén waves (Alfvén 1977).

In the terrestrial magnetotail, the magnetic reconnection serves as the fundamental plasma process to explosively convert magnetic energy to the plasma, which becomes the energy source of the FAC during the magnetosphere–ionosphere (M–I) coupling

processes (Vasyliunas 1975; Fu et al. 2017). Magnetic reconnections led to the generation of bursty bulk flows (BBFs; Angelopoulos et al. 1994; Nakamura et al. 2002) and dipolarization fronts (DFs; Sitnov et al. 2009; Fu et al. 2013). DFs, characterized by step-like enhancements of the northward magnetic field  $B_z$  (Ge et al. 2008, 2011; Runov et al. 2011a), play an important role in flux and energy transport (Angelopoulos et al. 2013; Liu et al. 2014). With Cluster and THEMIS observations, DFs are proposed to couple the magnetosphere and the ionosphere with strong field-aligned currents (Runov et al. 2011b). And the strong ultralow-frequency (ULF) waves within the Pi2 band produced by DFs (Panov et al. 2014a, 2014b) can connect the magnetotail source region with the ionosphere through FACs, which has been observed by magnetospheric spacecraft and ground stations (Panov et al. 2013; Keiling et al. 2014).

Multiple satellite programs for the Earth's magnetosphere and ionosphere facilitate our study of Earth's ionosphere and magnetosphere coupling. These coupled observations provide us with more theoretical support when dealing with magnetospheric observations on other planets. Using simultaneous observations from Cluster and Swarm, Dunlop et al. (2015) reported the clear matching of the behavior and structure of the large-scale currents. However, due to the small spatial scale and fast convection speed of DFs, simultaneous observations for tail DFs and their ionospheric effects remain absent. For other planets, we usually only obtain the magnetospheric or ionospheric observations at a single point.

<sup>6</sup> Corresponding author: Dr. Yasong Ge, Institute of Geology and Geophysics, Chinese Academy of Sciences.

In this Letter, we report the first-time direct conjugated observations from MMS and Swarm during a DF event and investigate the coupling of DF-driven ULF waves and ionospheric FACs. With high-resolution and multi-spacecraft measurements, we demonstrate that the ULF waves in the plasma sheet transport energy toward the ionosphere along the magnetic field lines through shear Alfvénic waves, which may evolve into kinetic Alfvén waves as they approach the ionosphere.

## 2. Instrumentation and Conjugated Observations

On 10 August 2017, a DF event was observed by MMS in the near-Earth region when the spacecraft were located at  $[-12.7, 2.6, 3.4] R_E$  in the geocentric solar magnetospheric (GSM) coordinates. Four MMS probes formed a tetrahedron configuration with about 10 km separation. FIELDS EDP (Ergun et al. 2016), Flux Gate magnetometer (Russell et al. 2016), and Fast Plasma Investigation (Pollock et al. 2016) data for particles are used in the present study. All the data are shown in the GSM coordinates unless noted otherwise.

Figure 1 shows the DF event observed by the MMS1 spacecraft from 14:55:00 to 15:15:00 UT, where the DF passed the spacecraft at around 15:05:45 UT. For simplicity, we only show the observations from MMS1 since the measurements from four probes are very similar due to small separations. The DF can be clearly identified by a sharp increase of the  $B_z$  component of the magnetic field from 5 nT to 20 nT within 5 s, accompanied by a similar enhancement of the magnetic field strength (Figure 1(a)). As shown in Figure 1(d), the elevation angle of the magnetic field increased from  $\sim 40^\circ$  to  $\sim 90^\circ$ . The background magnetic field strength was about 7 nT and the plasma beta value (the ratio of the plasma pressure to the magnetic pressure) was greater than 1, indicating that MMS1 was close to the neutral sheet (Cao et al. 2006). This DF was accompanied by a fast earthward flow over  $300 \text{ km s}^{-1}$  with a comparable dawn-ward flow. At the DF location, the proton and electron number densities suddenly dropped corresponding to the  $B_z$  enhancement (Figure 1(g)), while the electron and ion fluxes clearly increased at the higher-energy channels to signal the plasma energized behind the front (Figures 1(h)–(k)).

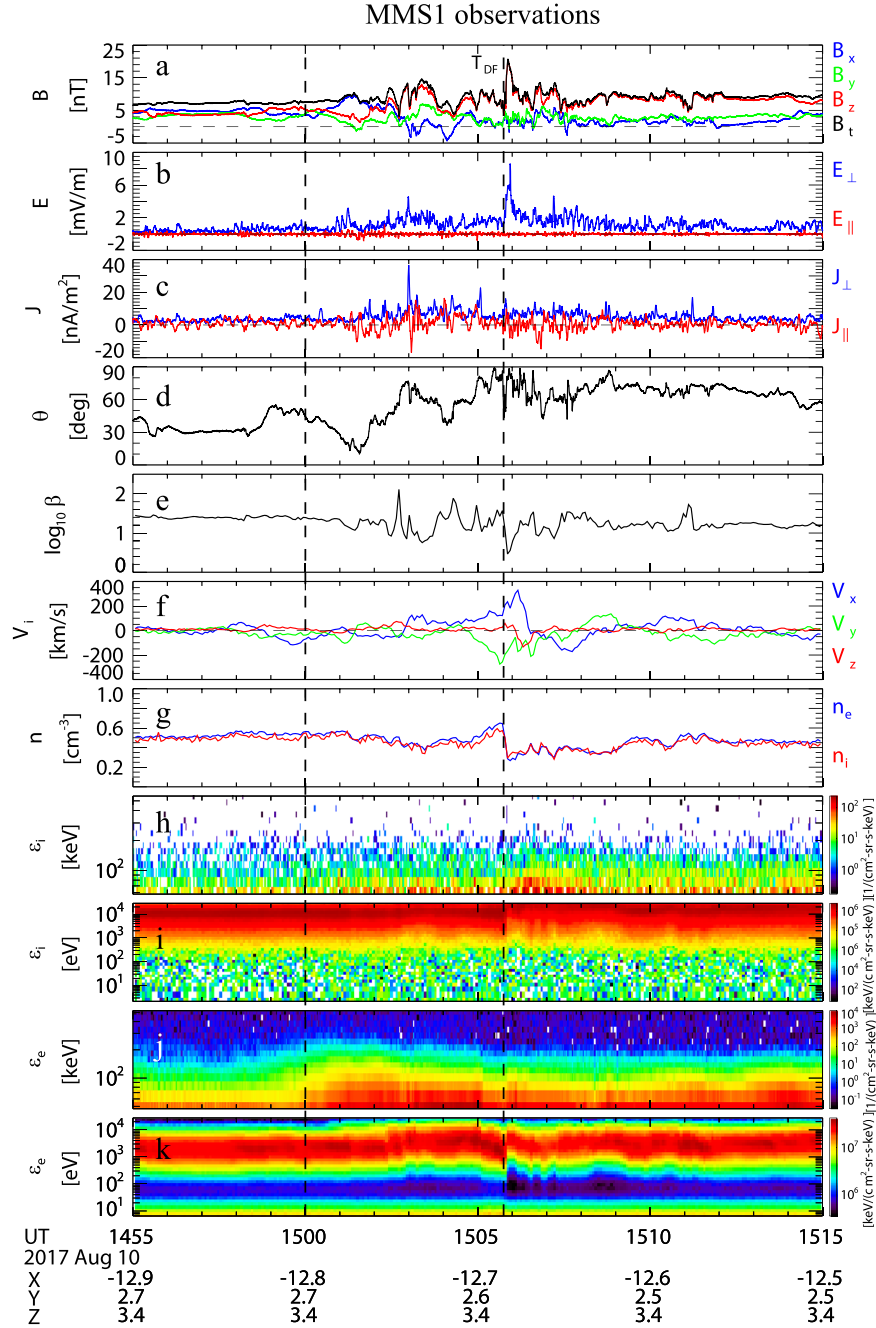
Prior to the DF arrival, large-amplitude fluctuations on all the components of the magnetic field were recorded by MMS spacecraft at 15:00:00 UT and lasted for 5 minutes until DF (marked by two dashed vertical lines in Figure 1). During the ULF waves prior to the DF, the variations on the particle density number and ions energy are rather subtle compared with those around the DF. It shows that during this interval the MMS spacecraft was located within a region where the properties of the plasma are different from those of the DF. During the magnetic fluctuations, substantial field-aligned currents occurred with a peak magnitude of  $\sim 18 \text{ nA m}^{-2}$  and showed changing directions relative to the local magnetic field (Figure 1(c)). To analyze the properties of the magnetic fluctuations in the compressional and transverse components, we have transformed the magnetic field data from GSM to the local mean field-aligned (MFA) coordinate system (Du et al. 2011).

Figure 2(a) shows the magnetic fluctuations prior to the DF in the MFA coordinates. The spectra of three magnetic field components in the MFA coordinates are obtained through the wavelet analysis, and the power spectrum density (PSD) during the strong magnetic fluctuations before the DF are also shown at the right of the wavelet spectra in Figures 2(b)–(d). The black traces in the wavelet spectra mark the local ion cyclotron

frequencies. Clearly, the perturbations on the background field direction dominate over other components. The dominant frequency of the magnetic fluctuations prior to the DF was  $\sim 5 \text{ mHz}$ , while there existed a clear second peak at  $\sim 15 \text{ mHz}$  for PSDs of the  $B_y$  and  $B_z$  components during the strong magnetic fluctuations. The wavelet spectra prior to the DF register the discrete wave power enhancement at 15 mHz on the  $B_y$  and  $B_z$  components during this 5 minute interval, which is within the frequency band of Pi2 waves (6–25 mHz). A bandpass filter with a frequency ranging from 12.5 mHz to 20 mHz is subsequently applied to the magnetic field fluctuations in the MFA coordinates. As shown in Figures 2(e)–(g), the large-amplitude Pi2-band oscillations of the magnetic field were mainly present for the  $B_y$  and  $B_z$  components, while the power for the  $B_x$  component was much smaller. As a consequence, prior to the DF the observed magnetic fluctuations showed comparable transversal and compressional components, while the compressional component dominated after the front. In Figure 2(h), using the magnetic field and electric field measurements from MMS, we show the parallel component of the Poynting flux ( $S_{\parallel}$ ) for the 12.5–20 mHz band magnetic waves during this DF event. As shown in Figure 1(a), the crossings of the neutral sheet by MMS were signaled by the  $B_x$  in GSM reversal several times. The shaded periods in Figure 2(h) indicated that MMS1 is located at the south lobe. It is found that when MMS was located in the northern (southern) hemisphere the parallel Poynting flux was positive (negative), indicating that the energy flux flowed along (against) the background field direction at north (south) of the neutral sheet. Thus, it is conceivable that the DF-driven Pi2-band waves transport the energy along the field line from the DF region toward the ionosphere.

The DF event occurred under relatively quiet solar wind conditions without strong geomagnetic activities (shown in Appendix A). By using the T96 model (Tsyganenko 1995) with the OMNI solar wind data, the magnetic footprints of MMS were located at the magnetic local time (MLT) of  $\sim 22.57$  and the magnetic latitude (MLAT) of  $\sim 64.57^\circ$  when the DF passed the spacecraft. Fortunately, we have the conjugate observations (discussed later) at the top of the ionosphere for this DF event because the Swarm spacecraft A and C passed the magnetic footprint region of the MMS spacecraft. The Swarm A and C, which flew side by side with a constant longitudinal separation of  $1.4^\circ$  and a time delay of about 7 s, passed through the MMS footprint region from poleward at an altitude of about 450 km.

Figure 3 shows the field-aligned current density calculated from the magnetic field observations by Swarm A and C. With the assumption that the current generally flows in the current sheets perpendicular to the magnetic meridian, we can obtain the field-aligned current from single-satellite measurements (Ritter et al. 2013). As shown in Figure 3(d), after a 7 s time shift, both Swarm spacecraft observed a pair of FAC sheets during 15:05:35 UT–15:06:40 UT, and FAC disturbances (shaded region) were observed in, actually almost overlapped with, the poleward-side FAC sheet. It can be seen from Figure 3(e) that the FAC sheet, which consist of two parts: downward (15:05:40 UT–15:06:10 UT) and upward (15:06:10 UT–15:06:45 UT) FACs, observed by Swarm A and C, with a small difference in longitude, were quite similar. The high correlation coefficient (i.e., 0.95) of large-scale currents from two spacecraft implies that the large-scale FACs



**Figure 1.** Encounter of MMS1 spacecraft with a DF event at  $(-12.7, 2.6, 3.4) R_E$  in the GSM coordinates from 1455 UT to 1515 UT on 2017 August 10. From top to bottom, (a) the  $B_x$  (blue),  $B_y$  (green),  $B_z$  (red), and the total magnitude of magnetic field (black) components of the magnetic field; (b) the parallel and perpendicular components of electric field; (c) the parallel and perpendicular components of current density; (d) the magnetic field elevation angle,  $\theta$ , defined as  $\theta = \tan^{-1}(B_z/(B_x^2 + B_y^2)^{1/2})$  (Yao et al. 2013); (e) plasma beta value,  $\beta$ ; (f)  $V_x$  (blue),  $V_y$  (green),  $V_z$  (red) components of ion flow velocity; (g) ion number density (red) and electron number density (blue); (h)–(k) proton and electron energy spectra. The second vertical dotted line denotes the start of the DF that arrived at MMS.

can be stationary. In addition, rapid FAC disturbances, and even reversed polarity of the FAC, can be observed by both A and C within 10 s. Furthermore, the FAC can be divided into two classes: small-scale FACs with sizes of up to around 10 km and large-scale FACs with sizes of more than 150 km in latitude (Lühr et al. 2015; Yang et al. 2018). From the correlation analysis, they obtained a persistent period of small-scale FACs of order 10 s, which is the temporal variation, while large-scale FACs can be regarded stationary for more than 60 s, which is the spatial variation. Thus, the stationary FACs sheet observed by Swarm A and C was supposed to be the large-

scale FAC, while the variational FAC disturbances were supposed to be the small-scale FAC.

It is worth noting that the FAC disturbances observed by Swarm C are much weaker; the density of the FAC was increased up to  $8 \mu\text{A m}^{-2}$  observed by Swarm A, while the peak current density increased up to  $3 \mu\text{A m}^{-2}$  observed by Swarm C only 7 s earlier. However, the small-scale FACs in general depend both on space and time (Forsyth et al. 2017). It is difficult to distinguish if the different observations of Swarm A and C were due to the temporal (7 s delay) or spatial variations (1.4 difference in longitude). One may speculate that

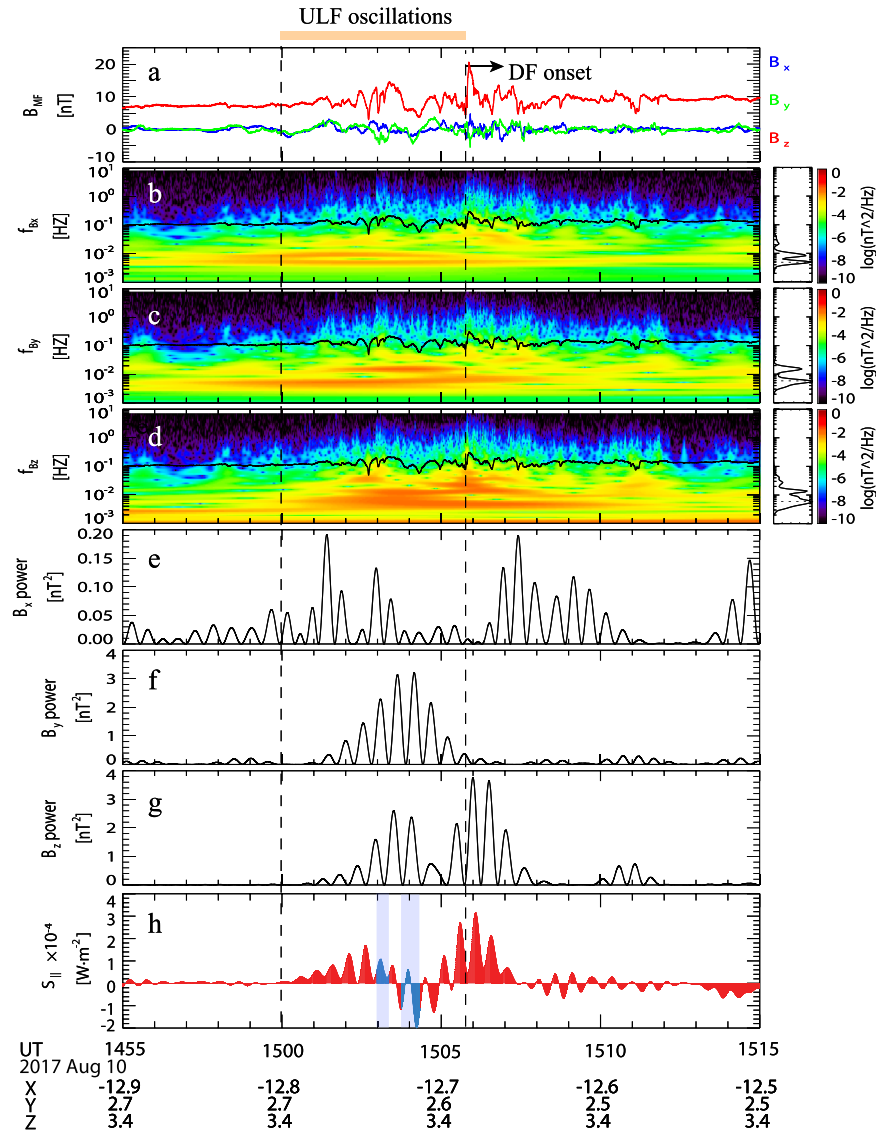


**Figure 2.** Power spectrograms of magnetic fields recorded by MMS1 in the frequency range (0.001–8) Hz. From top to bottom, (a) magnetic field in the MF coordinate; (b)–(d) the power spectrogram of the three components of the magnetic field, i.e.,  $B_z$ ,  $B_y$  and  $B_x$ , obtained via wavelet analysis in the MFA coordinate. The overlapped black trace shows the ion cyclotron frequency in each frequency–time spectrogram. The mean power spectra between the two vertical black dashed lines are calculated and displayed on the right side of the wavelet panel. (e)–(g) The power of the three components of the magnetic field, i.e.,  $B_x$ ,  $B_y$ , and  $B_z$ ; (h) field-aligned Poynting flux ( $S$ ) obtained using the magnetic and electric fields within the frequency band of 50–80 s. The shaded periods indicate that MMS1 is located at the south lobe ( $B_x$  in GSM is negative). At other times, the satellites are basically located in the north lobe. The interval between the two vertical dashed lines indicates the period of ULF magnetic oscillations.

these small-scale FAC structures are more filamentary rather than sheet-like (Lühr et al. 2015). Although, the calculation of the value of the small-scale FAC density is imprecise due to the lower applicability of the infinite current sheet approximation to the small-scale FAC. The fast-varying nature of the small-scale FAC observed by Swarm A and C can still be well reflected.

There was no obvious large-scale FAC observed farther poleward, suggesting that the small-scale FAC was located close to the poleward edge of the auroral oval. Generally, the small-scale FACs are associated with “short-lived” plasma processes within the magnetosphere such as discrete auroral arcs (Anderson & Vondrak 1975), field-line resonances (Rankin et al. 1999), bursty bulk flows in the plasma sheet (Yu et al. 2017), and associated Pi2 (Cao et al. 2008). We trace magnetic field lines, which are at the peak value of the small-scale FAC (well in the

close field lines), back to the magnetotail with the T96 model. The Swarm A and C are located at  $(-15.10, 0.07, 3.4)R_E$  and  $(-12.23, 0.29, 3.38)R_E$ , respectively. The DF event observed by MMS is located at  $(-12.7, 2.6, 3.4)R_E$ . By considering that the ULF fluctuations last  $\sim 5$  minutes before the DF arrivals and the ambient convection speed is  $\sim 200 \text{ km s}^{-1}$  (Figure 1; before it arrives at  $X = \sim -12 R_E$ ), the disturbed region covers  $\sim 9 R_E$  in the X-direction. Meanwhile, given that the DF width in Y is typically  $1\text{--}3 R_E$  (Nakamura et al. 2014), the backward tracing results show a good correspondence between Swarm and MMS.

### 3. Discussion

During the earthward propagation of DFs, different types of wave activity can be excited, while among these waves ULF waves may carry the most intense energy due to their typically



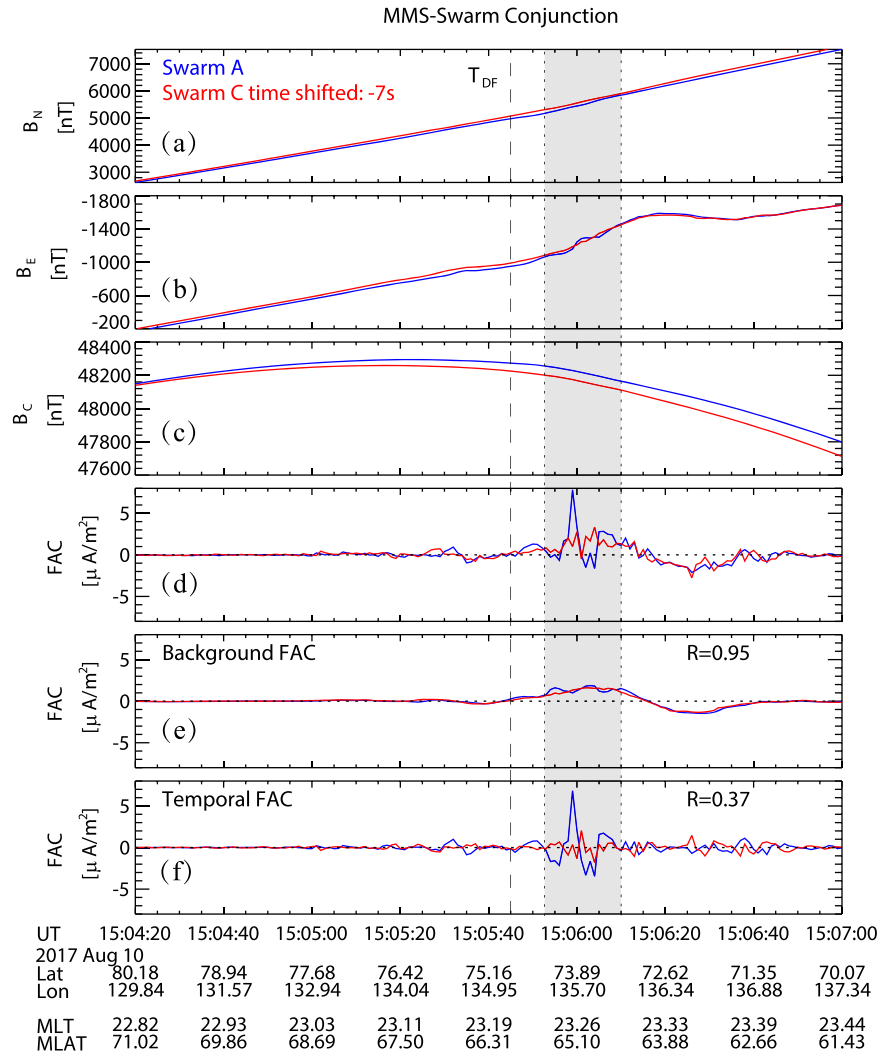


**Figure 3.** Swarm A and C observations from 15:04:20 UT to 15:07:00 UT on 2017 August 10. The footprint of MMS was located at  $\sim$  MLT 22.57,  $\sim$  MLAT  $64^{\circ}57'$ . The shaded region indicates the small-scale FAC region. Swarm A observations are shown in blue, while  $-7$  s time-shifted Swarm C observations are shown in red. From top to bottom, (a)–(c)  $B_N$ ,  $B_E$ , and  $B_C$  in the North–East–Centre (NEC) frame; (d) Swarm A and C observations of FACs; (e) the background FACs; and (f) the temporal FACs. The vertical dashed line (TDF) denotes the start of the DF that arrived at the MMS.

largest amplitudes. In this study, the DF event occurred under a relatively quiet solar wind condition (shown in Appendix A), and the MMS spacecraft was located within the braking region of DFs (Fu et al. 2012). The DF braking process, caused by the interaction between DFs and the strong magnetic field closer to the Earth, usually can produce compressional pulses as the direct driver of the low-latitude ground Pi2 pulsations (Kepko et al. 2001) and of Pi2-band waves in the plasma sheet (Wang et al. 2015). Kepko et al. (2001) described three separate paths for the Pi2 signal contained in the flows to propagate to the ground. Two paths involve compress mode waves, generated by the decelerating flow bursts, that reach the flanks and the low-latitude nightside region; the third path involves field-aligned currents also generated by decelerating flow bursts. Previously reported DF-driven ULF waves that can even penetrate inside the geosynchronous orbit (Runov et al. 2014; Liu et al. 2017) are consistent with the first two paths. In the present study the large-amplitude Pi2-band fluctuations immediately prior to the DF observed by MMS are consistent with the third path.

In this study, the Pi2-band power of magnetic fluctuations has a substantial transverse component comparable to the

compressional component driven by the DF braking. The compressional component immediately prior to the front shows its slow-mode nature as the plasma pressure and magnetic pressure perturbations are out of phase (shown in Appendix B), which is consistent with previous observations from Geotail, Cluster, and THEMIS (Nakamizo 2003; Wang et al. 2016). The comparable transverse component of magnetic fluctuations indicates the coupling of the slow-mode and shear Alfvén mode, which is confirmed by the parallel Poynting flux toward the ionosphere. Behind the DF, the transverse component becomes very small and the compressional component dominates, telling us that the DF also acts as a transition site where the wave mode is converted. This result is similar to the wave mode conversion event observed by the THEMIS spacecraft during the substantial change of the tail magnetic field inclination (Du et al. 2011). Here the transverse waves are likely generated by the DF-driven slow-mode waves, which usually occur when the diamagnetic current associated with the slow-mode flows along the inhomogeneous and curved magnetic field lines (Nakamizo 2003).

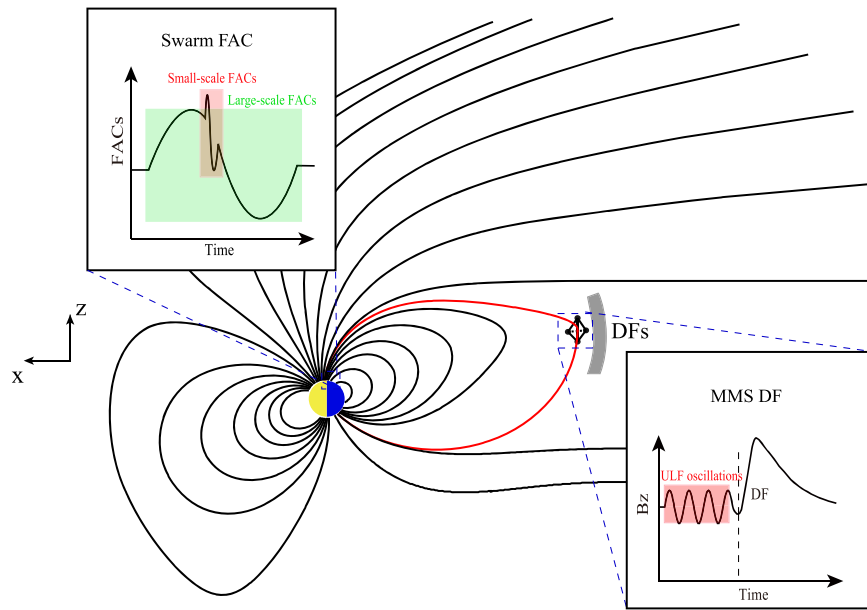


**Figure 4.** Cartoon illustrating the coupling between the DF and ionospheric small-scale FAC. The transverse mode of Pi2-like waves observed by MMS occur before the DF and travel along the magnetic field line toward Earth. These Pi2-like waves further evolve into kinetic Alfvén waves (KAWs) in the high-latitude magnetosphere, the latter of which can consequently drive the small-scale FACs in the ionosphere.

With the assumption that along a flux tube the magnetic flux and the particle flux are conserved and the flow speed is constant (Kan et al. 2011), the estimated traveling time of shear Alfvén waves from the plasma sheet near the MMS spacecraft to the location of Swarm spacecraft is about 108.2 s, which is consistent with the time delay from the peak of plasma sheet Alfvén waves (15:04:00 UT) to the ionospheric small-scale FACs (15:05:59UT). During the period of ULF wave activities, we find the consistence between the ionospheric currents and the magnetotail FACs (i.e., nature of transverse waves) through the conjugate observations of Swarm and MMS. When we map the plasma sheet FACs into the ionosphere, the current density increases from  $20 \text{ nA m}^{-2}$  measured by the MMS spacecraft to about  $10 \mu\text{A m}^{-2}$  in the ionosphere, which agrees with the peak current density measured by the Swarm spacecraft. Interestingly, within the large-scale ionosphere FACs there are small-scale current structures that exhibit temporal variations. This type of temporal ionospheric FAC, i.e., small-scale FACs (of the temporal order of 10 s), is generally thought to be associated with kinetic Alfvén waves (KAWs; Stasiewicz et al. 2000; Lühr et al. 2015). KAWs have a component of the electric field parallel to the ambient magnetic field and that can, therefore, accelerate electrons into the ionosphere. Moreover, these KAWs over the polar region may locally heat electrons through the Ponderomotive Force, and the heated electrons can cause a magnetic cavity through the diamagnetic effect (Dasgupta & Tsurutani 2003; Tsurutani et al. 2003). These small-scale, localized electromagnetic disturbances are often correlated with small-scale, discrete auroral arcs (Stasiewicz et al. 2000).

A recent 2.5-D hybrid simulation study of Guo et al. (2015) has found that the shear Alfvén waves caused by the earthward penetration of tail fast flows can evolve into KAWs in the high-latitude magnetotail when propagating toward the ionosphere along the magnetic field lines. The transition is attributed to the nonuniformity of the high-latitude magnetic field and density in the polar region. Stawarz et al. (2017) also reported that the KAWs with earthward energy flux were observed within the

plasma sheet but likely are near the boundary at a geocentric distance of  $9 R_E$  in association with bulk flow signatures.

For this DF event the solar wind condition was normal and there was no substorm activity according to the Auroral-Electrojet (AE) index. However, the Pi2-band waves and the FACs in both the magnetotail and the ionosphere presented significant similarity to those associated with magnetospheric substorms. It has been proposed that the current system, including FACs that connect the tail and the ionosphere, around magnetotail DFs may form a “wedgelet” in each DF, and a substorm current wedge (SCW) may be built from multiple DF “wedgelets” (Liu et al. 2015; Yao et al. 2015). The relationship of SCW and multiscale FACs during magnetotail DFs is outside the scope of this study and left to future investigation.

#### 4. Conclusions

The magnetotail DFs can drive different types of plasma waves and generate a 3D current system around the fronts during their fast convection through the tail plasma sheet. To investigate the connection to and influence upon the ionosphere of such tail dynamics, space-ground conjugate observations are necessarily required but rarely implemented. This Letter adopts high-quality measurements from the Swarm and MMS spacecraft and manifests the conjugated observations of DF-driven Pi2-band waves and FACs that connect the tail DF and ionospheric currents.

Figure 4 illustrates our findings with a cartoon. On 2017 August 10, a plasma sheet DF event was observed by the MMS spacecraft and was preceded by 5 minutes of large-amplitude ULF magnetic fluctuations. The waves have the power mainly within the Pi2 band and consist of comparable compressional and transverse (shear Alfvén waves) components of magnetic oscillations. Although the associated FACs change their directions during the Pi2-band waves, the Poynting flux of the transverse mode oscillations reveals that the DF-driven ULF waves caused earthward energy flux along the magnetic

field lines. The corresponding FACs were also observed by the Swarm A and C spacecraft near the magnetic footprint of the MMS spacecraft during this event. The ionospheric FAC was found to have small-scale structures with fast temporal variations that are usually associated with KAWs. We conclude that the braking of tail DF and BBF causes the preceding Pi2-band waves with a significant transverse component. These ULF waves subsequently propagate into the ionosphere along the magnetic field lines and contribute to the formation of small-scale temporal FACs and the evolution of KAWs.

We thank the Magnetospheric Multiscale (MMS) Science Data Center (SDC) for providing MMS magnetic field and plasma data and the ESA Swarm project for Swarm data. All data are open access and can be downloaded at <https://lasp.colorado.edu/mms/sdc> and <https://earth.esa.int/web/guest/swarm/data-access>. This work is supported by the National Key Research and Development Program of China (2016YFB0501304, 2016YFB0501300), the National Natural Science Foundation of China (grant Nos. 41774176, 41874080, 41674168, 41974173), the Strategic Priority Research Program of Chinese Academy of Sciences (grant Nos. XBD41010300, XDA14040404), the pre-research Project on Civil Aerospace Technologies No. D020103 funded by CNSA and the Youth

Innovation Promotion Association, Chinese Academy of Sciences.

## Appendix A Geomagnetic Conditions

With OMNI data, the solar wind and interplanetary magnetic field (IMF) conditions on 2017 August 10 are shown below. On 15:05 UT when the MMS observed the DF, the IMF  $B_Y$  and  $B_Z$  components are 3.31 nT and 0.74 nT, respectively, and the IMF was mostly northward around the DF. The solar wind dynamic pressure is about 1.31 nPa and the solar wind velocity  $V_x$  component is about  $-400 \text{ km s}^{-1}$ . The AE index stays around 80 nT and the AL index around  $-25 \text{ nT}$ , the SYM\_H is about  $-2 \text{ nT}$ . Those conditions indicated that this DF event occurred under relatively quiet solar wind conditions without strong geomagnetic activities.

## Appendix B Slow-mode Nature of ULF Oscillations prior to DF

Figure A1 shows the magnetic field and plasma observations of MMS during the DF event. The bandpass filter with the upper frequency of 0.02 Hz and lower frequency of 0.0125 Hz is chosen to cover the dominant frequency (1/65 Hz) of the magnetic

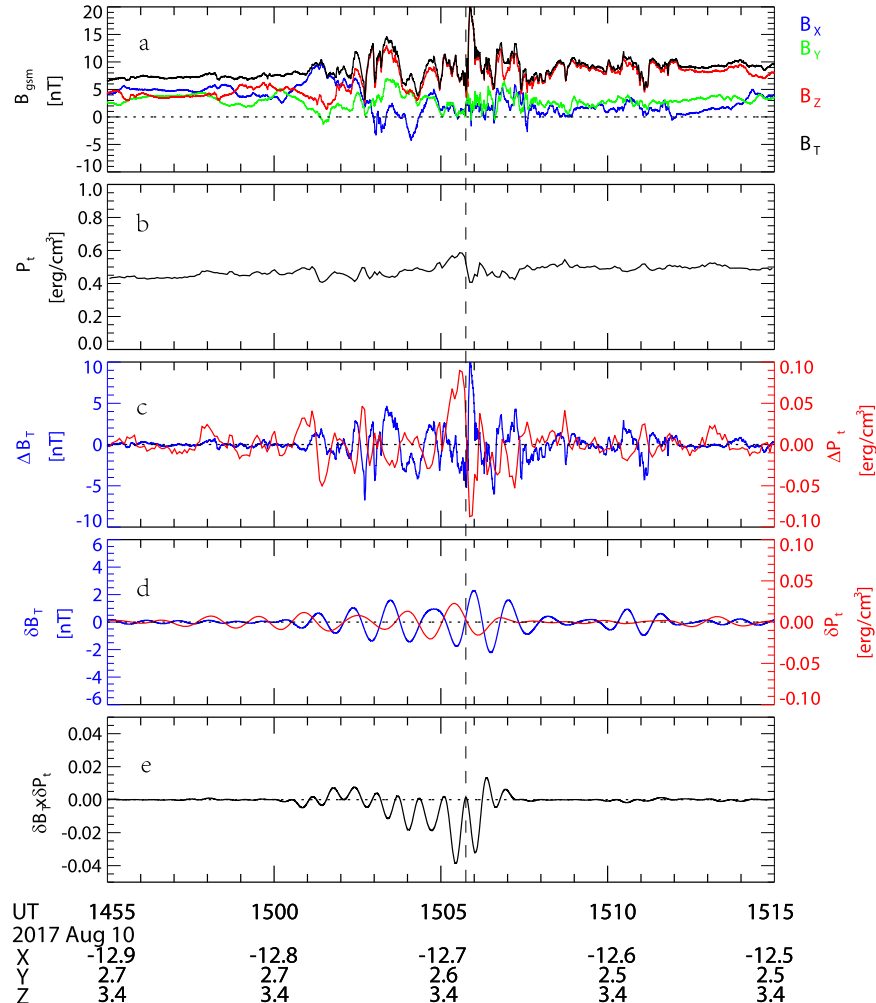


**Figure A1.** (a) The magnetic field components and magnitude observed by MMS1, (b) the plasma pressure, (c) the variations of the magnetic field strength  $\Delta B_T$  and the plasma pressure  $\Delta P_t$ , (d) the filtered fluctuations of the magnetic field strength  $\delta B_T$ , and the plasma pressure  $\delta P_t$ , through the bandpass filter [50–80 s]. (e) The product of  $\delta B_T$ ,  $\delta P_t$ . The dashed vertical line marks the DF onset time.

fluctuations around the DF. Figure A1(c) shows the variations of the magnetic field strength  $\Delta B_T$  and the plasma pressure  $\Delta P_t$  around the dipolarization region, and Figure A1(d) shows the [50-80 s] filtered fluctuations of the magnetic field strength  $\delta B_T$  and the plasma pressure  $\delta P_t$ . Figure A1(e) shows the product of  $\delta B_T \delta P_t$ , which is mostly negative. It indicated that the waves observed prior to the DF are predominantly the slow MHD waves.

### ORCID iDs

Pengfei Qin  <https://orcid.org/0000-0002-2402-3405>  
 Yasong Ge  <https://orcid.org/0000-0002-4345-522X>

### References

- Alfvén, H. 1977, *RGSP*, **15**, 271
- Anderson, B. J., Korth, H., Waters, C. L., et al. 2014, *GeoRL*, **41**, 3017
- Anderson, H. R., & Vondrak, R. R. 1975, *RvGSP*, **13**, 243
- Angelopoulos, V., Kennel, C. F., Coroniti, F. V., et al. 1994, *JGR*, **99**, 21257
- Angelopoulos, V., Runov, A., Zhou, X. Z., et al. 2013, *Sci.*, **341**, 1478
- Bagenal, F. 2007, *JASTP*, **69**, 387
- Cao, J., Duan, J., Du, A., et al. 2008, *JGRA*, **113**, A07S15
- Cao, J. B., Ma, Y. D., Parks, G., et al. 2006, *JGRA*, **111**, A04206
- Cowley, S. W. H. 2000, in *Magnetospheric Current Systems*, Geophysical Monograph 118, ed. S. Ohtani et al. (Washington, DC: AGU), 91
- Dasgupta, B., & Tsurutani, B. T. 2003, *GeoRL*, **30**, 2128
- Delamere, P. A. 2003, *JGRA*, **108**, 1276
- Du, J., Zhang, T. L., Nakamura, R., et al. 2011, *GeoRL*, **38**, L07101
- Dunlop, M. W., Yang, J. Y., Yang, Y. Y., et al. 2015, *GeoRL*, **42**, 3683
- Ergun, R. E., Tucker, S., Westfall, J., et al. 2016, *SSRv*, **199**, 167
- Forsyth, C., Rae, I. J., Mann, I. R., et al. 2017, *JGRA*, **122**, 3411
- Fu, H. S., Cao, J. B., Khotyaintsev, Y. V., et al. 2013, *GeoRL*, **40**, 6023
- Fu, H. S., Khotyaintsev, Y. V., Vaivads, A., et al. 2012, *GeoRL*, **39**, L10101
- Fu, H. S., Vaivads, A., Khotyaintsev, Y. V., et al. 2017, *GeoRL*, **44**, 37
- Ge, Y. S., Raeder, J., Angelopoulos, V., et al. 2011, *JGRA*, **116**, A00I23
- Ge, Y. S., Russell, C. T., & Hsu, T. S. 2008, *AdSpR*, **41**, 1243
- Guo, Z. F., Hong, M. H., Lin, Y., et al. 2015, *PhPI*, **22**, 022117
- Kan, J. R., Li, H., Wang, C., et al. 2011, *AnGeo*, **29**, 2045
- Keiling, A., Marghitu, O., Vogt, J., et al. 2014, *JGRA*, **119**, 2717
- Kepko, L., Kivelson, M. G., & Yumoto, K. 2001, *JGR*, **106**, 1903
- Liu, J., Angelopoulos, V., Chu, X. N., et al. 2015, *GRL*, **42**, 1669
- Liu, J., Angelopoulos, V., Zhang, X. J., et al. 2017, *JGRA*, **122**, 10112
- Liu, J., Angelopoulos, V., Zhou, X.-Z., et al. 2014, *JGRA*, **119**, 909
- Lühr, H., Park, J., Gjerloev, J. W., et al. 2015, *GeoRL*, **42**, 1
- Mauk, B. H., Anderson, B. J., & Thorne, R. M. 2002, in *Atmospheres in the Solar System: Comparative Aeronomy*, Geophysical Monograph 130, ed. M. Mendillo, A. Nagy, & J. H. Waite (Washington, DC: AGU), 97
- Mcpheeron, R. L., Russell, C. T., & Aubry, M. P. 1973, *JGR*, **78**, 3131
- Nakamizo, A. 2003, *JGRA*, **108**, 1286
- Nakamura, R., Baumjohann, W., Runov, A., et al. 2002, *GeoRL*, **29**, 2140
- Nakamura, R., Karlsson, T., Hamrin, M., et al. 2014, *GeoRL*, **41**, 777
- Panov, E. V., Baumjohann, W., Kubyskhina, M. V., et al. 2014a, *JGRA*, **119**, 6603
- Panov, E. V., Baumjohann, W., Nakamura, R., et al. 2013, *JGRA*, **118**, 1529
- Panov, E. V., Baumjohann, W., Nakamura, R., et al. 2014b, *JGRA*, **119**, 4512
- Pollock, C., Moore, T., Jacques, A., et al. 2016, *SSRv*, **199**, 331
- Rankin, R., Samson, J. C., & Tikhonchuk, V. T. 1999, *GeoRL*, **26**, 663
- Ritter, P., Luhr, H., & Rauberg, J. 2013, *EP&S*, **65**, 1285
- Runov, A., Angelopoulos, V., Sitnov, M., et al. 2011a, *P&SS*, **59**, 517
- Runov, A., Angelopoulos, V., Zhou, X. Z., et al. 2011b, *JGRA*, **116**, A05216
- Runov, A., Sergeev, V. A., Angelopoulos, V., et al. 2014, *JGRA*, **119**, 1643
- Russell, C. T., Anderson, B. J., Baumjohann, W., et al. 2016, *SSRv*, **199**, 189
- Russell, C. T., Khurana, K. K., Kivelson, M. G., et al. 2000, *AdSpR*, **26**, 1499
- Saur, J., Neubauer, F. M., & Connerney, J. E. P. 2004, in *Jupiter. The planet, satellites and magnetosphere*, ed. F. Bagenal, T. E. Dowling, & W. B. McKinnon (Cambridge: Cambridge Univ. Press), 537
- Sitnov, M. I., Swisdak, M., & Divin, A. V. 2009, *JGRA*, **114**, A04202
- Stasiewicz, K., Bellan, P., Chaston, C., et al. 2000, *SSRv*, **92**, 423
- Stawarz, J. E., Eastwood, J. P., Varsani, A., et al. 2017, *GeoRL*, **44**, 7106
- Tsurutani, B. T., Dasgupta, B., Arballo, J. K., et al. 2003, *NPGeo*, **10**, 27
- Tsurutani, B. T., Lakhina, G. S., & Hajra, R. 2020, *NPGeo*, **27**, 75
- Tsyganenko, N. A. 1995, *JGR*, **100**, 5599
- Vasyliunas, V. M. 1975, *RvGSP*, **13**, 303
- Wang, G. Q., Ge, Y. S., Zhang, T. L., et al. 2015, *JGRA*, **120**, 6167
- Wang, T., Cao, J., Fu, H., et al. 2016, *GeoRL*, **43**, 1854
- Yang, J. Y., Dunlop, M. W., Luhr, H., et al. 2018, *JGRA*, **123**, 8170
- Yao, Z. H., Liu, J., Owen, C. J., et al. 2015, *AnGeo*, **33**, 1301
- Yao, Z. H., Sun, W. J., Fu, S. Y., et al. 2013, *JGRA*, **118**, 6980
- Yu, Y. Q., Cao, J. B., Fu, H. S., et al. 2017, *JGRA*, **122**, 6139